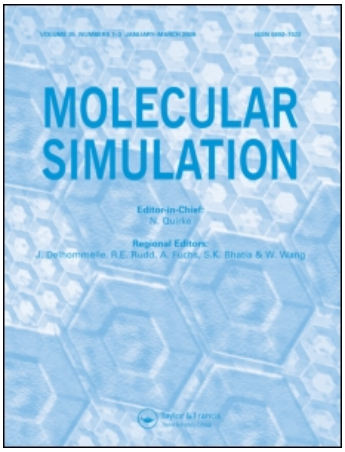

Molecular Simulation
Publication details, including instructions for authors and subscription information:
http://www.informaworld.com/smpp/title~content=t713644482

Non Equilibrium Molecular Dynamics Simulation of Coupled Heat- and Mass Transport Across a Liquid/Vapor Interface

Bjørn Hafskjold[ab]; Tamio Ikeshoji[ac]
[a] Cluster Science Group, National Institute for Advanced Interdisciplinary Research, Tsukuba, Ibaraki, Japan [b] Department of Physical Chemistry, University of Trondheim - Norwegian Inst. of Technology, TRONDHEIM, Norway [c] Tohoku National Industrial Research Institute, Sendai, Japan

To cite this Article Hafskjold, Bjørn and Ikeshoji, Tamio(1996) 'Non Equilibrium Molecular Dynamics Simulation of Coupled Heat- and Mass Transport Across a Liquid/Vapor Interface', Molecular Simulation, 16: 1, 139 — 150
To link to this Article: DOI: 10.1080/08927029608024068
URL: http://dx.doi.org/10.1080/08927029608024068

Molecular Simulation, 1996, Vol. 16, pp. 139–150
Reprints available directly from the publisher
Photocopying permitted by license only

NON EQUILIBRIUM MOLECULAR DYNAMICS SIMULATION OF COUPLED HEAT- AND MASS TRANSPORT ACROSS A LIQUID/VAPOR INTERFACE

BJØRN HAFSKJOLD[1] and TAMIO IKESHOJI[2]

Cluster Science Group, National Institute for Advanced Interdisciplinary Research, 1-1-4, Higashi, Tsukuba, Ibaraki 305, Japan

(Received March 1995, accepted May 1995)

The transport properties of bulk liquid, gas and at the gas/liquid interface were studied for two binary Lennard-Jones/spline mixtures by use of nonequilibrium molecular dynamics. One of the mixtures was an ideal isotope mixture, the other a non-ideal mixture. The simulations gave the thermal conductivity, mutual diffusion coefficient, heat flux, mass flux, and the changes in these quantities across the interface. The local entropy production was expressed in terms of fluxes and thermodynamic forces, and numercial estimates are given. It was shown that the largest contribution to the total entropy production occurs in the vapor phase under the chosen conditions. We expect, however that if the mass flux were larger, the major contribution to the entropy production would come from the liquid phase.

KEY WORDS: Heat flux, mass flux, interface, nonequilibrium molecular dynamics, entropy production.

1 INTRODUCTION

Heat and mass transfer across an interface occurs frequently in natural and industrial processes, such as in crystallization and distillation. The phase transition causes dramatic changes not only in the thermodynamic properties, such as the density, and in the local structure, but also in the transport coefficients and the molecular mechanisms for the transport processes. For instance, the diffusion coefficient and thermal conductivity change by 4 and 2–3 orders of magnitude, respectively, from liquid to vapor [1]. If there is a mass flux present, the heat flux across the interface will also change, due to the fact that the heat of vaporization represents a source term in the heat balance equation. These transport processes are in principle coupled, as given formally by the equations of irreversible thermodynamics [2] (shown here for a binary system without viscous flow, using the mean molar velocity

[1] On leave of absence from Department of Physical Chemistry, University of Trondheim–Norwegian Inst. of Technology, N-7034 TRONDHEIM, Norway.

[2] On leave from Tohoku National Industrial Research Institute, 4-2-1, Nigatake, Miyagino-ku, Sendai, 983, Japan

as frame of reference),

$$\vec{J}_q = -l_{qq}\frac{\vec{\nabla} T}{T^2} - l_{q1}\frac{\vec{\nabla}_T(\mu_1 - \mu_2)}{T} \tag{1}$$

$$\vec{J}_1^m = -l_{1q}\frac{\vec{\nabla} T}{T^2} - l_{11}\frac{\vec{\nabla}_T(\mu_1 - \mu_2)}{T} \tag{2}$$

In equations (1) and (2), $\vec{J}_q$ and $\vec{J}_1^m$ are the measurable heat flux and the molar flux of component 1, respectively, $\vec{\nabla}T$ is the temperature gradient, and $\vec{\nabla}(\mu_1 - \mu_2)$ is the gradient in chemical potential of component 1 relative to that of component 2. The coefficients l_{ij} are phenomenological coefficients. The coupling, *i.e.* the relation between the heat flux and the chemical potential gradient (the Dufour effect) and between the mass flux and the temperature gradient (the Soret effect), is normally weak in bulk phases, and heat- and mass transfer are usually treated as separate processes [3]. At the interface, however there will be a strong, direct coupling between the heat- and mass fluxes through the heat of vaporization, analogous to the heat of melting in frost heave [4]. To what extent the Dufour and Soret effects contribute to the heat- and mass transfer across an interface is not known on the basis of experimental results.

We shall in this work study a liquid/vapor interface by nonequilibrium molecular dynamics (NEMD), because this will provide us with a lot more detailed information than the thermodynamic results. However, the relationship between the molecular and thermodynamic descriptions of a two-phase system with an interface is not trivial, and we shall in this work limit ourselves to the computational aspects of the problem for simple model fluids. In particular, we will consider one ideal and one non-ideal binary mixture of Lennard-Jones/spline particles. The conditions will be chosen such that the system separates into a liquid and a vapor phase.

In previous papers, we have established NEMD algorithms that generate heat- and mass fluxes [5–7]. The algorithms were mostly applied to studies of the Soret effect in supercritical, binary isotope mixtures [8, 9], but in one case we generated a liquid drop with a heat sink in the center, surrounded by vapor with a heat source at the perimeter of the MD cell [6]. A slightly different geometry of the system and of the heat source and -sink will establish a planar interface.

Studies of interfaces by computer simulations are not new. Rao and Levesque [10] generated a two-phase system by a setting up the initial configuration with a liquid slab surrounded by vapor. This method has been found to give two-phase equilibrium systems that are stable over a sufficiently long time for time averages to be calculated [11, 12]. The present study differs from the previous ones in that two external forces are applied, a temperature gradient and a chemical potential gradient. For any initial configuration, the system will then fall into a state with two coexisting phases if the thermodynamic variables for the total system are chosen appropriately, and it will reach a stationary state that can be used to compute averages. Local equilibrium prevails even under extremely large forces [7,13–15], and the nonequilibrium system may also be conveniently used to set up initial configurations for equilibrium studies of the interface and two-phase coexistence [16].

The question we address here is how the thermodynamic forces and fluxes vary across the interface. We will also study how the molecular mechanisms for heat transport vary, and where the entropy is produced under different conditions. In this paper, we will focus on the simulation aspects of these questions, whereas the thermodynamic aspects and implications for distillation will be discussed in a forthcoming paper [17].

The formal relations we need from irreversible thermodynamics are given in Section 2 of this paper. The model system and the simulations are described in Section 3. In Section 4, we analyse the results of the simulations in terms of the thermodynamic formalism, and show for instance how local values for the fluxes and the entropy production can be obtained. The conclusions are given in Section 5.

2 FORMAL RESULTS FROM IRREVERSIBLE THERMODYNAMICS

The flux-force relations in equations (1) and (2) stem from the following expression for the local entropy production rate per unit volume in the binary mixture [2]

$$\theta = -\vec{J}_q \frac{\vec{\nabla} T}{T^2} - \sum_{i=1}^{2} \vec{J}_i \frac{\vec{\nabla}_T \mu_i}{T} \tag{3}$$

and the assumption that the fluxes are linearly related to the forces. In distillation, the separation of the components is of primary interest. One way to express the rate of separation is by the separation flux, $\vec{J}_d^m$, defined as [18]

$$\vec{J}_d^m = \frac{\vec{J}_1^m}{x_1} - \frac{\vec{J}_2^m}{x_2} \tag{4}$$

where x_i is the mole fraction of component i. Introducing equations (1), (2), and (4) into equation (3), using that $\vec{J}_1^m = -\vec{J}_2^m$ and some recombination, gives an alternative expression for the entropy production:

$$\theta = \lambda \left(\frac{\vec{\nabla} T}{T} \right)^2 + \frac{(x_1 x_2)^2}{l_{11}} (\vec{J}_d^m)^2 \tag{5}$$

where the thermal conductivity is defined by

$$\lambda = \left(l_{qq} - \frac{l_{1q} l_{q1}}{l_{11}} \right) \frac{1}{T^2} \tag{6}$$

The diffusion coefficient, D, is defined through the relation [2]

$$\vec{J}_1^m = -nD \vec{\nabla} x_1 \tag{7}$$

at isothermal conditions. In equation (7), n is the molar density.

In this work, we will focus on the separation flux, the heat flux, the thermal conductivity, the diffusion coefficient, and the entropy production.

3 THE NEMD SIMULATIONS

The MD cell contained a binary mixture of 2048 particles. The cell was non-cubic with sides $L_x/8 = L_y = L_z$ and it had normal periodic boundary conditions.

A description of how the coupled heat- and mass transport was generated is given elsewhere [6, 7]. In brief, the cell was divided into 64 layers of equal thickness perpendicular to the x-axis as shown in Figure 1. To generate a heat flux, layers no. 1 and 64 (counting from one end of the box) were thermostatted to a high temperature T_H, and layers 32 and 33 (in the center of the box) were thermostatted to a low temperature T_L. The thermostatting was made with a simple rescaling of the velocities, subject to momentum conservation [6, 7]. The high-temperature and low-temperature regions will be referred to as regions H and L, respectively. This gave a symmetry plane in the center of the cell, consistent with the periodic boundary conditions. In the layers between regions H and L (shown as M in Fig. 1), the particles obeyed the normal Newtonian equations of motion, and these regions were used for computing the stationary-state averages. This way of thermostatting the system is very similar to the method used by Tenenbaum *et al.* [13] and Ashurst and Hoover [19]. In addition to giving a heat flux from the hot ends to the cold center of the cell, the temperature profile also generated a liquid region in the center with one vapor region at each side.

Fickian mass diffusion was generated by particle swapping from type 2 to type 1 in region H and simultaneously from type 1 to type 2 in region L. This gave a surplus of type 1 particles in region H and of type 2 in region L, with a consequent diffusive mass flux in between. This particle swapping method is similar to that used by Sindzingre *et al.* [20].

Since the external forces that drove the system out of equilibrium were applied at narrow regions in the system, this method is a *boundary-driven* NEMD method. Because these regions are thin layers perpendicular to the x-axis, the fluxes and forces are one-dimensional (in the x-direction).

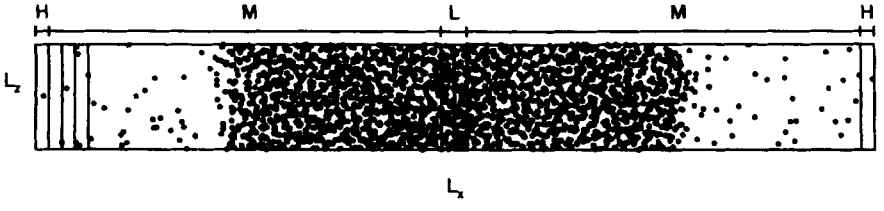

Figure 1 Projection of the NEMD cell in the x-z plane. The cell is divided into 64 layers perpendicular to the x-axis, but only 7 of the layers are shown here. The particles of component 1 are drawn as black circles and component 2 are shown as white circles. The particles are not drawn to scale, the molecular diameter σ is approximately equal to the thickness of one layer.

The particles interacted with the Lennard-Jones/spline potential [21],

$$u_{ij}(r) = \begin{cases} 4\varepsilon_{ij}\left[\left(\frac{\sigma_{ij}}{r}\right)^{12} - \left(\frac{\sigma_{ij}}{r}\right)^{6}\right] & \text{for } r \leqslant r_s \\ a_{ij}(r-r_c)^2 + b_{ij}(r-r_c)^3 & \text{for } r_s \leqslant r \leqslant r_c \\ 0 & \text{for } r \geqslant r_c \end{cases} \tag{8}$$

where $r_s = (26/7)^{1/6}\,\sigma_{ij}$, $r_c = (67/48)r_s$, $a_{ij} = -(24192/3211)\,\varepsilon_{ij}/r_s^2$, and $b_{ij} = -(387072/61009)\varepsilon_{ij}/r_s^3$. The parameters σ_{ij} and ε_{ij} represent the molecular diameters and intermolecular potential depths, respectively.

Instead of the heat flux, we compute the local, instantaneous internal energy flux $\vec{J}_U$ in each layer of the MD cell according to Evans and Morriss [22]:

$$\vec{J}_U = \frac{1}{V}\sum_{i \in CV}\left(\left[\frac{1}{2}m_i(\vec{v}_i - \vec{v})^2 + \phi_i\right](\vec{v}_i - \vec{v}) - \frac{1}{2}\sum_{\substack{j=1 \\ j \neq i}}^{N}[(\vec{v}_i - \vec{v})\cdot\vec{F}_{ij}]\,\vec{r}_{ij}\right) \tag{9}$$

where V is the volume of each layer (each control volume CV), m_i and $\vec{v}_i$ are the mass and velocity, respectively, of particle i, $\vec{v}$ is the barycentric velocity of the system, ϕ_i is the potential energy of particle i in the field of all the other particles, $\vec{F}_{ij}$ is the force acting on i due to j, $\vec{r}_{ij}$ is the vector from the position of i to the position of j, and N is the total number of particles in the system. The internal energy flux was also computed from the amount of energy added and withdrawn from regions H and L, respectively, during the thermostatting.

The heat flux is related to the internal energy flux by

$$\vec{J}_q = \vec{J}_U - \sum_{k=1}^{2} H_k \vec{J}_k \tag{10}$$

where H_k is the partial molar enthalpy of component k.

The results from the NEMD simulations are reported in reduced Lennard-Jones units, *i.e.* reduced number density, $n^* = N\sigma_{11}^3/V$, reduced temperature, $T^* = k_B T/\varepsilon_{11}$, reduced mass, $m^* = m/m_1$, reduced energy flux, $J_U^* = J_U(\sigma_{11}^3/\varepsilon_1)\,(m_1/\varepsilon_{11})^{1/2}$, and reduced mass flux $J_i^* = J_i(\sigma_{11}^3/m_1)\,(m_1/\varepsilon_{11})^{1/2}$. The phase diagram of this system is to some extent known [23], and we chose the overall temperature and density in such a way that we got about equal volumes of vapor and liquid in the cell.

Three cases were studied: (1) isotope (ideal) mixture with heat- and mass flux, (2) non-ideal mixture with heat flux, and (3) non-ideal mixture with heat- and mass flux. The isotope mixture had a mass ratio $m_2/m_1 = 0.1$. The non-ideal mixture had the following parameters: $m_2/m_1 = 1$, $\varepsilon_{22}/\varepsilon_{11} = \varepsilon_{12}/\varepsilon_{11} = 0.8$, and $\sigma_{22}/\sigma_{11} = \sigma_{12}/\sigma_{11} = 1.0$. The composition of the ideal mixture was $z_1 = 0.5$, whereas the non-ideal mixture had $z_1 = 0.8$, where z is the overall mole fraction. In all three cases, the mean molar velocity was zero ($\vec{J}_1^m = -\vec{J}_2^m$), T_H and T_L were set to 1.0 and 0.7, respectively, and the overall number density was 0.4. The mass flux imposed by the particle swapping is given in Table 1.

Table 1 Values for the fluxes and forces in reduced Lennard-Jones units.

Case	$J_U^* \times 10^3$	$J_q^* \times 10^3$	$J_1^* \times 10^3$	$\nabla T_{vap}^* \times 10^3$	$\nabla T_{liq}^* \times 10^3$	$\nabla x_{1,vap}^* \times 10^3$	$\nabla x_{1,liq}^* \times 10^3$
1	1.989	1.989	0.340	−11.2	−0.441	−1.59	−2.84
2	3.274	3.274	0	−11.2	−0.874	1.61	0.94
3	2.703	–	0.409	−10.9	−0.985	−3.62	−9.80

For each case, 3.6×10^6 time steps of length $\delta t^* = 0.002$ each were generated. The first 0.6×10^6 time steps were allowed for stabilizing the stationary state, and the rest were used for computing the averages.

4 RESULTS AND DISCUSSION

In Case 1, since $\vec{J}_1^m = -\vec{J}_2^m > 0$, and the mixture is an isotope mixture, the heat of vaporization of component 2 exactly cancelled the heat of condensation of component 1. Consequently, there was no heat source at the interface, and $\vec{J}_q$ was constant throughout the system at stationary state. The isotope mixture will have a positive thermal diffusion factor, which means that the lighter component will migrate towards the hot side if there is no initial concentration gradient [5,9]. The Soret effect will therefore contribute to the demixing, although the effect is negligibly small compared to the Fickian diffusion [9] caused by the imposed concentration gradient in this case. For Case 2, there was a separation dominated by the equilibrium coexistence compositions, with a surplus of the more volatile component (2) in the vapor phase, overlayed by the Soret effect. Again, the Soret effect was likely to be small. In this case, the mass fluxes were zero, and for this reason there was no heat source at the interface so that $\vec{J}_q$ was independent of x. The particle swapping in Case 3 had an additional demixing effect as it moved some of the less volatile component 1 particles from the liquid to the vapor. Even though $\vec{J}_1^m = -\vec{J}_2^m$, the two components now had different heats of vaporization, and $\vec{J}_q$ varied throughout the system (due to the heat of mixing) and especially across the interface (due to the heat of vaporization). The configuration shown in Figure 1 is actually for Case 3, and the composition profile can be seen, especially in the liquid.

The reduced temperature is shown as function of x/L_x in Figure 2 for all three cases. The total temperature difference between regions H and L was set by the thermostats to be 0.3 in all cases. Due to the lower thermal conductivity in the vapor than in the liquid, about 95% of the total temperature difference occurs in the vapor phase. The temperature drop through the vapor is therefore also almost fixed as shown by Figure 2. Variations in the thermal conductivity of the vapor from one system to another will therefore show up in the heat flux rather than in the temperature gradient. The temperature is continuous across the interface, even in Case 3 with a strong heat source at the interface.

The density profile in Figure 3 shows an interface region that extends over 5–8 molecular diameters in all cases (one molecular diameter is approximately the thickness of one layer), in good agreement with earlier works on the interface of Lenneard-Jones systems [10–12, 24]. The isotope mixture shows a slightly higher liquid

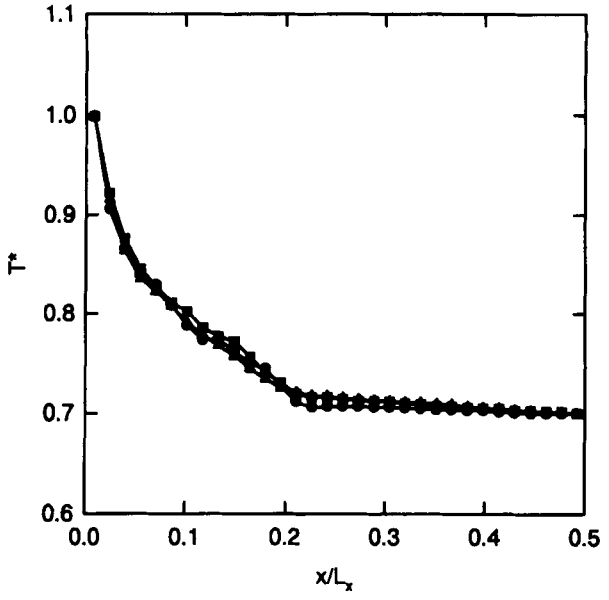

Figure 2 Temperature profile across one half of the cell. (The values from the left and right halves were pooled). The symbols are: ● Case 1, ■ Case 2, ▲ Case 3.

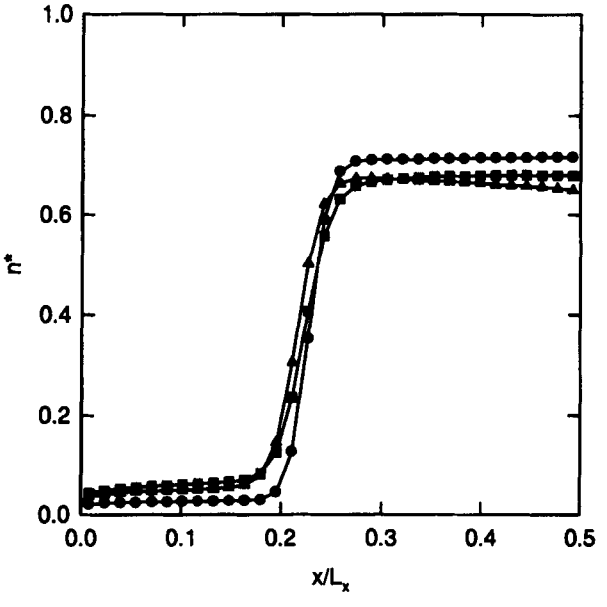

Figure 3 Density profile across one half of the cell. The symbols are: ● Case 1, ■ Case 2, ▲ Case 3.

density and a lower vaopor density, and consequently a larger change in volume on vaporization. Because some 20% of the particles in the non-ideal liquid mixture have weaker attractive forces than in the isotope mixture (overall mole fraction of component 2 equals 0.2), the liquid density of the non-ideal mixture is smaller. Weaker attractive

forces in the liquid gives higher volatility, and consequently the non-ideal mixture has a higher vapor density than the isotope mixture at the same temperature.

The results for the fluxes and forces are given in Table 1. The vapor has much higher resistance to heat flow than the liquid, and its conductivity is a limiting factor for the heat flow. The thermal conductivity is shown in Table 2. The heat flux is higher for the non-ideal mixture than for the ideal mixture, which must be attributed to the non-ideal mixture's higher density (and consequently higher thermal conductivity) in the vapor phase. We have not computed $\vec{J}_q$ in Case 3 because we do not have data for the partial molar enthalpies. The ideal *liquid* mixture has a somewhat higher thermal conductivity than the non-ideal mixture. In terms of equation (9), this can be understood from the term involving $\vec{F}_{ij}$ (the collision term). The weaker interactions in the non-ideal mixture give smaller contributions to the collision term. The terms involving the kinetic and potential energies contribute very little [8].

The mole fraction profiles are shown in Figure 4. The fact that the isotope mixture is an ideal mixture leads to no change in composition from liquid to vapor, other than the composition gradient imposed by the particle swapping, which gives

Table 2 Densities, transport coefficients, and activity coefficients. The densities and the mole fractions used for computing the activity coefficients were extrapolated to the interface from the profiles in the bulk phases.

Case	n^*_{vap}	n^*_{liq}	λ^*_{vap}	λ^*_{liq}	D^*_{vap}	D^*_{liq}	$\gamma_{1,liq}$	$\gamma_{2,liq}$
1	0.030	0.707	0.178	4.51	7.13	0.169	1.00	1.00
2	0.075	0.661	0.292	3.75	–	–	0.64	2.64
3	0.059	0.680	–	–	1.91	0.061	0.72	3.72

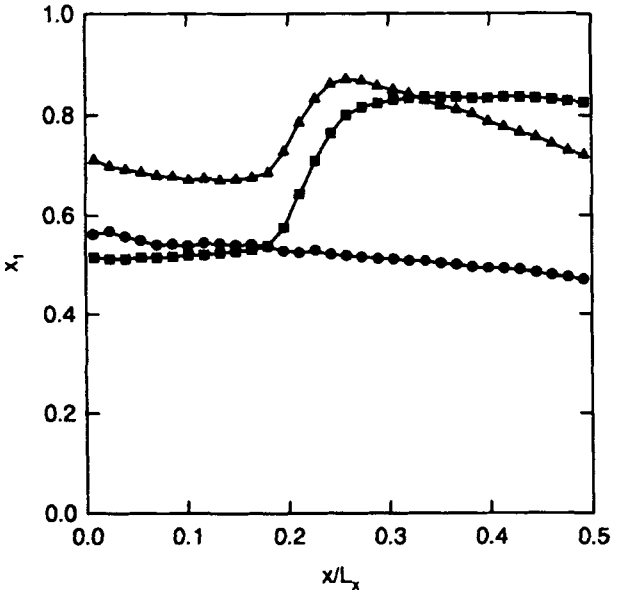

Figure 4 Mole fraction shown as function of x. The symbols are: ● Case 1, ■ Case 2, ▲ Case 3.

rise to the mass flux. The non-ideal system has a change of about 0.3 mole fraction units across the interface. Assuming ideal gas and local equilibrium at the interface, we can then compute the activity coefficient in the liquid as

$$\gamma_i = \frac{y_i}{x_i} \tag{11}$$

where y_i and x_i are the mole fractions of component i in vapor and liquid, respectively. The results are given in Table 2, which also includes our estimates for the mutual diffusion coefficient. In all cases, the mole fraction gradients are of the same order of magnitude, but the diffusion coefficient is much smaller in the liquid.

For Case 2 we can estimate the thermal diffusion factor, α_{12}, defined by

$$\vec{\nabla} \ln(x_1/x_2) = -\alpha_{12} \vec{\nabla} \ln T \tag{12}$$

We found $\alpha_{12} \approx 5.3$ for the liquid phase and $\alpha_{12} \approx 0.4$ for the vapor near the interface ($T^* = 0.75$). The liquid value is substantially higher than what has been found previously for the similar, but equimolar Kr/Ar mixture [8,14,15], probably due to the difference in composition.

The separation flux, $\vec{J}_d^m$, is shown in Figure 5 for Cases 1 and 3. The abrupt change at the interface for Case 3 is due to the change in equilibrium composition from liquid to vapor, and the slopes in bulk liquid and vapor are due to the mole-fraction gradient caused by the particle swapping. The larger composition gradient in the liquid is reflected here in a steeper slope in $\vec{J}_d^m$ in the liquid than in the vapor.

The entropy production profile was computed from Equation 3, and the results are shown in Figure 6 for Cases 1 and 2. For Case 1, the contribution from the mass flux

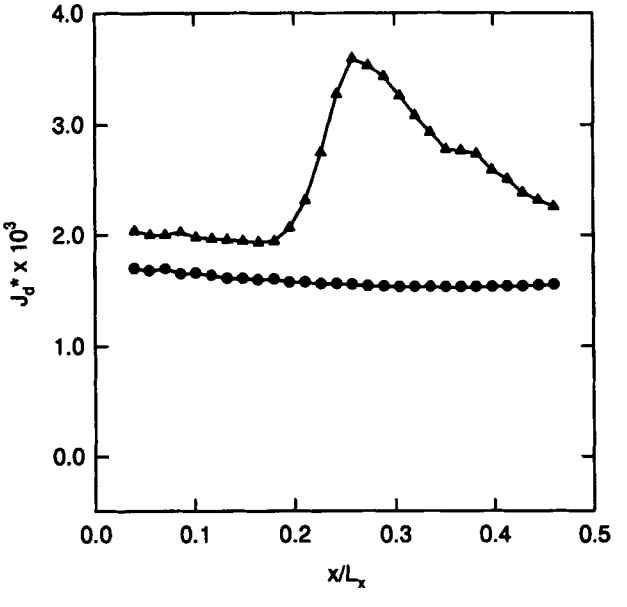

Figure 5 The difference mass flux, $\vec{J}_d^m$ in one half of the cell and across the interface. The symbols are: ● Case 1, ▲ Case 3.

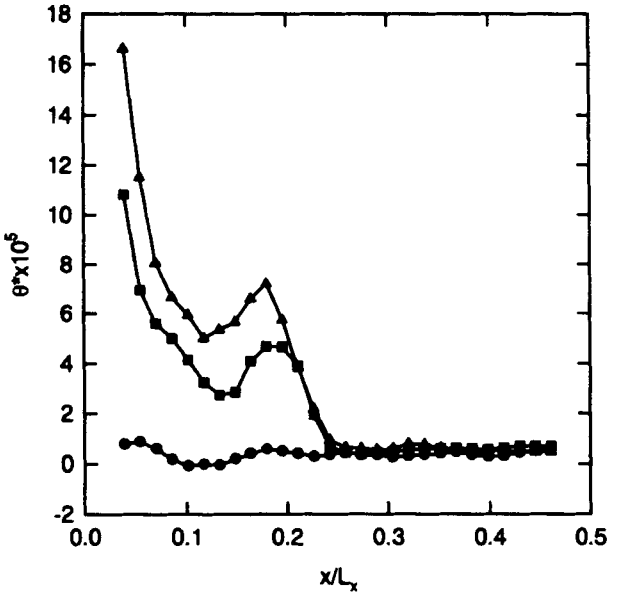

Figure 6 Entropy production profile across one half of the cell. The symbols are: ● mass flux contribution from Case 1, ■ total entropy production, Case 1, ▲ total entropy production, Case 2.

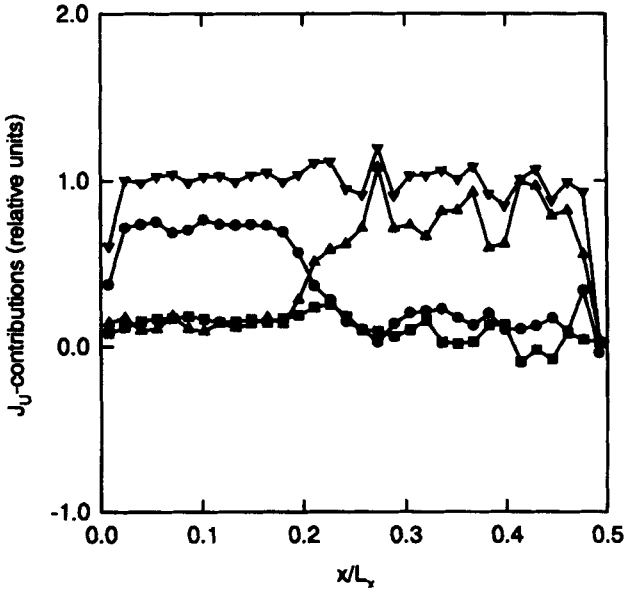

Figure 7 Relative contributions to the internal energy flux, Case 2. "Relative" means J_U computed from Equation (9) divided by the value computed from the energy input and withdrawal from regions H and L during thermostatting. The symbols are: ● Kinetic energy flux, ■ Potential energy flux, ▲ Intermolecular energy transfer (collision energy), ▼ Total.

(the second term in Equation (3)) is very small, and the total entropy production is dominated by the first term (not shown in the figure). For Case 2, the mass-flux contribution is zero. The larger entropy production in the non-ideal system (Case 2) is due to the larger heat flux in this system because the vapor phase is more thermally conductive. In both cases, almost all the entropy production occurs in the vapor phase, but it can not be drawn as a general conclusion that this will always be the case, because the relative contributions are given by how the heat- and mass fluxes are set. The reason for the peak in the entropy production close to the interface is not clear; it is related to the weak shoulder in the temperature profile (see Fig. 2).

The internal energy flux (Equation (9)), may be divided into three different contributions, a kinetic energy contribution, a potential energy contribution, and a collision term. The relative contributions are shown in Figure 7 for Case 2. The most dominant features in the change from vapor to liquid are: (1) The kinetic energy flux is large in the vapor phase (due to the large mean free path) and small in the liquid phase, (2) the potential energy flux is small everywhere, like in the isotope mixtures studied previously [8], and (3) the collision energy is large in the liquid (due to strong interactions) and small in the vapor.

5 CONCLUSIONS

Two-phase systems with heat- and mass transport across a vapor/liquid interface were in this work generated by NEMD. An isotope mixture and a non-ideal mixture where the two components had the same molecular mass and diameter, but different potential depths were studied. For both systems, we found that the interface thickness was some 5–8 molecular diameters. The activity coefficients in the non-ideal liquid was determined from the vapor-phase composition, assuming ideal mixture in the gas phase. The transport properties were determined in the liquid and vapor bulk phases. The heat flux and the separation flux showed a strong variation across the interface.

The entropy production per unit volume was found to be much larger in the vapor than in the liquid, but this cannot be drawn as a general conclusion as it depends on the relative magnitudes of the heat- and mass fluxes.

Across the interface, there is a dramatic change in the molecular mechanisms for heat transport. The dominant mechanism in the vapor phase is flux of kinetic energy, whereas energy transfer through molecular interactions dominates in the liquid.

Acknowledgements

BH thanks The Agency of Industrial Science and Technology (AIST) and The Norwegian Inst. of Technology for financial support to stay at The National Institute for Advanced Interdisciplinary Research, Japan. Computer resources at The Research Information Processing System of AIST was greatly appreciated.

References

[1] R. C. Reid, J. M. Prausnitz, and T. K. Sherwood, *The properties of gases and liquides*, 3rd. ed., MCGraw-Hill, New York (1977).

[2] S. R. de Groot and P. Mazur, *Non-equilibrium thermodynamics*, Dover Ed., New York (1984).

[3] R. Taylor, R. Krishnamurthy, J. S. Furno, and R. Kroshna, "Condensation of vapor mixtures. 1. Nonequilibrium models and design procedures", *Ind. Eng. Chem. Process Des. Dev.*, **25**, 83 (1985).

[4] K. S. Førland, T. Førland, and S. K. Ratkje, *Irreversible Thermodynamics. Theory and Applications*, Wiley, Chichester (1988).

[5] J. M. Kincaid, X. Li, and B. Hafskjold, "Nonequilibirum molecular dynamics calculation of the thermal diffusion factor", *Fluid Phase Equil.*, **76**, 113–121 (1992).

[6] T. Ikeshoji and B. Hafskjold, "Non-equilibrium molecular dynamics calculation of heat conduction in liquid and through liquid-gas interface", *Molec. Phys.*, **81**, 251–261 (1994).

[7] B. Hafskjold and S. K. Ratkje, "Criteria for local equilibrium in a system with transport of heat and mass", *J. Stat. Phys.*, **78**, 463–493 (1995).

[8] B. Hafskjold, T. Ikeshoji, and S. K. Ratkje, "On the molecular mechanism of thermal diffusion in liquids", *Molec. Phys.*, **80**, 1389–1412 (1993).

[9] J. M. Kincaid and B. Hafskjold, "Thermal diffusion factors for the Lennard-Jones/spline system", *Molec. Phys.*, **82**, 1099–1114 (1994).

[10] M. Rao and D. Levesque, "Surface structure of a liquid film", *J. Chem. Phys.*, **65**, 3233–3236 (1976).

[11] M. Rao and B. J. Berne, "On the location of surface tension in the planar interface between liquid and vapour". *Molec. Phys.*, **37**, 455–461 (1979).

[12] M. J. P. Nijmeijer, A. F. Bakker, C. Bruin, and J. H. Sikkenk, "A molecular dynamics simulation of the Lennard-Jones liquid-vapor interface", *J. Chem. Phys.*, **89**, 3789–3792 (1988).

[13] A. Tenenbaum, G. Ciccotti, and R. Gallico, "Stationary nonequilibrium states by molecular dynamics. Fourier's law", *Phys. Rev.*, **A25**, 2778–2787 (1982).

[14] D. MacGowan, and D. J. Evans, "Heat and matter transport in binary liquid mixtures", *Phys. Rev.*, **A34**, 2133–2142 (1986).

[15] G. V. Paolini and G. Ciccotti, "Cross thermotransport in liquid mixtures by nonequilibrium molecular dynamics", *Phys. Rev.*, **A35**, 5156–5166 (1987).

[16] B. Hafskjold and R. Halseid, "Phase diagram for the Lennard-Jones/spline system", (in preparation).

[17] S. K. Ratkje and B. Hafskjold, "Entropy production rates in distillation of binary mixtures" (in preparation).

[18] S. K. Ratkje, E. Sauar, E. Kristiansen, K. M. Lien, and B. Hafskjold, "Analysis of entropy production rates for design of distillation columns" I & EC Res., **34**, 3001–3007 (1995).

[19] W. T. Ashurst and W. G. Hoover, "Dense-fluid shear viscosity via nonequilibrium molecular dynamics" *Phys. Rev.*, **A11**, 658–678 (1975).

[20] P. Sindzingre, C. Massobrio, G. Ciccotti, and D. Frenkel, "Calculation of partial enthalpies of an argon-krypton mixture by *NPT* molecular dynamics", *Chem. Phys.*, **129**, 213–224 (1989).

[21] B. L. Holian and D. J. Evans, "Shear viscosities away from the melting line: A comparison of equilibrium and nonequilibrium molecular dynamics", *J. Chem. Phys.*, **78**, 5147–5150 (1983).

[22] D. J. Evans and G. P. Morriss, *Statistical mechanics of nonequilibrium liquids*, in *Theoretical Chemistry*, ed. by D. P. Craig and R. McWeeny, Academic Press, London (1990).

[23] R. Halseid, *The critical point of the Lennard-Jones spline fluid*, Project Report, Norw. Inst. of Technology (1993).

[24] M. J. Haye and C. Bruin, "Molecular dynamics study of the curvature correction to the surface tension", *J. Chem. Phys.*, **100**, 556–559 (1994).